

Optimal Day-ahead Scheduling of Islanded Microgrid Considering Risk-based Reserve Decision

Zehuai Liu, Siliang Liu, Qinhao Li, Yongjun Zhang, Wenyang Deng, and Lai Zhou

Abstract—Due to the lack of support from the main grid, the intermittency of renewable energy sources (RESs) and the fluctuation of load will derive uncertainties to the operation of islanded microgrids (IMGs). It is crucial to allocate appropriate reserve capacity for the economic and reliable operation of IMGs. With the high penetration of RESs, it faces both economic and environmental challenges if we only use spinning reserve for reserve support. To solve these problems, a multi-type reserve scheme for IMGs is proposed according to different operation characteristics of generation, load, and storage. The operation risk due to reserve shortage is modeled by the conditional value-at-risk (CVaR) method. The correlation of input variables is considered for the forecasting error modeling of RES and load, and Latin hypercube sampling (LHS) is adopted to generate the random scenarios of the forecasting error, so as to avoid the dimension disaster caused by conventional large-scale scenario sampling approaches. Furthermore, an optimal day-ahead scheduling model of joint energy and reserve considering risk-based reserve decision is established to coordinate the security and economy of the operation of IMGs. Finally, the comparison of numerical results of different schemes demonstrate the rationality and effectiveness of the proposed scheme and model.

Index Terms—Day-ahead scheduling, risk-based reserve decision, conditional value-at-risk (CVaR), renewable energy source (RES), islanded microgrids.

I. INTRODUCTION

THERE is an extensive consensus that the exploitation and utilization of renewable energy sources (RESs) are one of the promising ways of solving environmental problems and resource crisis. According to the prediction of [1], RESs represented by wind turbine (WT) and photovoltaic (PV) will become the largest source of global power genera-

tion by 2040. Energy transition is also a significant issue for China. Chinese Energy Production and Consumption Revolution Strategy (2016-2030), issued by Chinese National Development and Reform Commission (NDRC) [2], sets a target that 50% of the power generation will be from non-fossil energy sources by 2030.

In order to tackle the significant increase of uncertainties caused by high penetration of RESs, exploiting the flexible resources from generation-load-storage side is the key to maintaining power balance in real time [3]. The microgrids (MGs), which are composed of distributed generation (DG), energy storage (ES) and flexible load, provide an effective technical means for the comprehensive utilization of RESs [4], [5]. According to whether connected to the main grid, MGs can be classified into grid-connected MGs and islanded MGs (IMGs) [6]. In remote areas without utility power grid coverage, IMG has become a good choice for electrical energy supply [7], [8], which can synthetically utilize local RESs and effectively reduce the cost of power supply.

Compared with grid-connected MGs, the operation of IMGs has the following salient features.

- 1) As an IMG receives little support from the main grid, it faces the challenge of power balance. The mismatch of generation and load will directly affect the operation reliability of IMG and the accommodation of RESs [7].
- 2) In respect of operation decision, it needs optimal scheduling of internal flexible resources for an IMG to manage and deal with uncertainties [8]. In general, compared with grid-connected MGs, IMGs are more sensitive to uncertainties considering the architecture and operation characteristics [7].

As a crucial aspect of MG scheduling, day-ahead scheduling is an important reference for coordinated operation of each unit in the next day [9]. In the context of high penetration of RESs, there is still a big gap between the day-ahead power forecasting and the real-time operation. Furthermore, the fluctuation of load will also further aggravate the operation uncertainties. It is necessary to consider the forecasting errors of RESs and load in the process of day-ahead scheduling. Since IMGs are more sensitive to uncertainties, reserve decision is the key segment of day-ahead scheduling for IMGs [10], [11]. In the day-ahead scheduling for IMGs considering the forecasting errors, the following two aspects need to be addressed: ① accurate modeling of forecasting er-

Manuscript received: February 26, 2020; accepted: August 17, 2020. Date of CrossCheck: August 17, 2020. Date of online publication: November 20, 2020.

This work was supported by the National Natural Science Foundation of China (No. 51777077) and the Natural Science Foundation of Guangdong Province (No. 2017A030313304).

This article is distributed under the terms of the Creative Commons Attribution 4.0 International License (<http://creativecommons.org/licenses/by/4.0/>).

Z. Liu, S. Liu, Q. Li, Y. Zhang (corresponding author), and L. Zhou are with the School of Electric Power, South China University of Technology, Guangdong Key Laboratory of Clean Energy Technology, Guangzhou, China, and Z. Liu is also with Dongguan Power Supply Bureau of Guangdong Power Grid Co., Ltd., Dongguan, China (e-mail: 464685495@qq.com; 463695442@qq.com; 872093413@qq.com; zhangjun@scut.edu.cn; 291666680@qq.com).

W. Deng is with Guangzhou Power Electrical Technology Co., Ltd., Guangzhou, China (e-mail: 775931271@qq.com).

DOI: 10.35833/MPCE.2020.000108



rors of RESs and load; ② reasonable reserve decision in day-ahead scheduling to deal with the operation risk arising from the forecasting errors.

To solve the former aspect, numerous studies have been undertaken to investigate the modeling of the forecasting errors of RESs and load. Normal distribution is widely used to model the uncertainties of forecasting errors [12]–[15]. In the existing studies, the forecasting error parameters of different types of RESs and load are mostly set independently. Thus, the influence of the complementarity of different RESs and the correlation between RES and load on the forecasting errors are not considered. Whereas, IMGs are independent small systems, which tend to present a correlation among different RESs and load, e.g., the complementarity of PV-WT, and the inverse peak characteristics of WT-load [16], [17]. The correlation between one RES and another RES and that between RES and load will fail to be reflected if the forecasting errors of different RESs and load are independently modeled. Therefore, it is necessary to consider the correlation for forecasting error modeling of RESs and load, so as to study and analyze the influence on the day-ahead scheduling of IMGs.

With regards to the latter aspect, reasonable reserve decision plays a fundamental role in optimal operation under uncertainties [18]. Three types of methods are generally used for reserve decision, which are deterministic methods, probabilistic methods, and risk-based methods. Deterministic methods usually allocate the positive and negative spinning reserve capacities in a certain proportion of peak load to cope with the forecasting errors of RESs and load [19], which have the advantages of simple model and low computational burden. However, the operation process of each reserve unit and whether they satisfy the power constraint remain to be further studied. Probabilistic methods can obtain the reserve decision schemes covering the probability space of random variables. They usually limit the system reliability indices to an artificial reliability level in the form of constraints (e.g., chance constraints) [14], [15], [20], [21], which is easy to ignore low-probability but high-risk events. Furthermore, probabilistic methods also lack the coordination between economy and reliability. Risk-based methods further evaluate the residual value of risk of the uncovered area, and adopt cost-benefit analysis to convert the system operation risk into the potential loss of lost load or RES power curtailment, so as to coordinate the economy and reliability [22]–[24].

Among several risk measures, value-at-risk (VaR) is a well-known measure focusing on the tail risk [25]. However, VaR is not a coherent risk measure and is difficult or even impossible to be calculated directly [26]. In contrast with VaR, conditional VaR (CVaR) is a coherent risk measure, which has the superiority in quantifying risks and mathematical properties such as convexity and differentiability [23], [27]. CVaR is widely used in risk measure and management for power system planning [28] and operation [29].

Nevertheless, there is little literature on the risk-based reserve decision for MGs. In [30], an optimal bidding strategy considering uncertainties of RES and demand response is proposed for grid-connected MGs. In the model, reserve and

penalty costs of incorrect estimation of RESs and risk of participation in the competitive energy market are assessed by using CVaR criteria. A model of joint energy and reserve scheduling by considering risk management for IMG is presented in [31], and uncertainties of RES, demand loads, and electricity prices are modeled by adopting CVaR. In [32], the risk of IMG operator in decision-making is controlled by CVaR, and then an operation formulation is proposed to simultaneously schedule energy and reserve with the aim of compensating for uncertainties.

According to the above literature survey, through the optimal scheduling of joint energy and reserve, the problem of reserve scheduling for MGs is solved to some extent. In respect of reserve schemes, the existing studies mainly focus on single spinning reserve schemes provided by dispatchable generators only [10], [19] and generation-load joint reserve schemes provided by dispatchable generators and interruptible load (IL) [31], [32]. However, the uncertainties of RESs and the fluctuation of load will lead to a significant increase in the reserve requirement of IMGs with high penetration of RESs. If the reserve capacity is provided by spinning reserve only, the operation economy will be deteriorated, and the original intention in developing RESs will be violated due to the emission of high proportion of spinning reserve. Whereas, making a large amount of responsive loads participate in auxiliary reserve through demand response will impact the power utilization experience and sacrifice the reliability to some extent. Therefore, it is of considerable significance for improving the economy and reliability of IMGs to fully tap various flexible resources and realize coordinated and complementary utilization of multi-type reserve capacities.

The major contributions of this paper are summarized as follows.

1) A generation-load-storage multi-type reserve scheme for IMGs is proposed, which can fully tap various flexible resources in MGs, and alleviate the shortage of flexibility regulation capacity caused by high penetration of RESs.

2) In view of the fact that the correlation of forecasting errors and its influence on IMG operation have not been fully studied, a model considering the forecasting errors of RESs and load with the correlation of input variables is presented to describe the probability distribution of day-ahead forecasting errors. Furthermore, Latin hypercube sampling (LHS) considering correlation is adopted to generate the random scenarios of forecasting errors, which can avoid the dimension disaster caused by conventional scenario sampling approaches such as Monte Carlo simulation (MCS), and the risk leakage caused by scenario reduction techniques.

3) A model of risk-based reserve decision is established, in which CVaR is employed to measure the potential loss of lost load and RES power curtailment caused by insufficient reserve. Subsequently, an optimal model of joint energy and reserve scheduling considering risk-based reserve decision is established. The proposed model can not only reasonably allocate reserve capacity to achieve risk aversion, but also improve the operation economy of IMGs.

The remainder of this paper is organized as follows. A multi-type reserve scheme for IMGs is proposed in Section

II. Subsequently, the reserve risk management by considering CVaR for IMG is presented in Section III. The LHS-based random scenario generation method considering the correlation is introduced in Section IV. The model of joint energy and reserve scheduling for IMGs is presented in Section V. Case studies together with simulation results are given in Section VI. Finally, conclusions are drawn in Section VII.

II. MULTI-TYPE RESERVE SCHEME FOR IMGs

The typical architecture of IMGs is shown in Fig. 1, where N-IL stands for non-interruptible load, MGC stands for MG controller, and DPDG stands for dispatchable DG. The MGC is mainly responsible for power forecasting and energy management. Unlike conventional distribution systems which mainly rely on DPDGs to provide spinning reserve, the flexibility resources for IMGs include ES and IL. Hence, a multi-type reserve scheme for IMG can be built from generation-load-storage side. In this paper, “multi-type” refers to various types of flexible resources [33], including DPDGs, ES, and IL. In addition, upward/downward reserve capacity is also regarded as upward/downward regulation capacity [34]. Upward regulation means that the schedulable units should increase their power output. On the contrary, downward regulation requires the schedulable units to decrease power output.

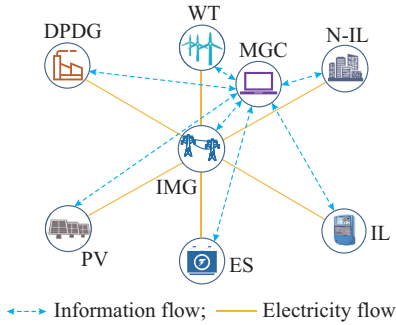


Fig. 1. Typical architecture of IMGs.

On generation side, the reserve capacity mainly depends on DPDGs such as microturbine (MT) and diesel generator. DPDGs can provide upward/downward reserve capacity by increasing/decreasing power output.

On storage side, the application of ES provides a richer means for IMG reserve, which is mainly undertaken by energy-type ES such as battery ES system. ES provides upward/downward reserve capacity via its charging/discharging.

On load side, the reserve mainly derives from the incentive-based demand response [31], [32]. Load shedding can be executed to provide upward reserve support for IMG when it reveals the insufficient power supply.

The generation-load-storage multi-type reserve scheme for IMGs is shown in Fig. 2. The reserve capacity provided by each type of equipment depends on its operation state, i.e., the power scheduling of each schedulable unit in IMGs will also impact its reserve capacity. According to the characteristics of each type of reserve capacity, the coordination and optimization of reserve capacity can give full play to the adapt-

ability and complementarity of each type of reserve capacity. Thus, the flexibility resources within IMGs are optimally allocated, which can alleviate the shortage of flexibility regulation capacity caused by high penetration of RESs.

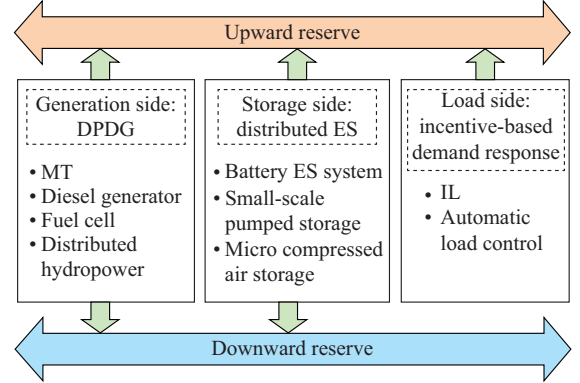


Fig. 2. Generation-load-storage multi-type reserve scheme for IMGs.

III. RISK-BASED RESERVE DECISION

The prominent function of flexibility resources for IMGs lies in providing instantaneous upward/downward reserve capacity during the actual operation, so as to reduce the operation risk (i.e., lost load or RES power curtailment) caused by uncertainties of RESs and load. In day-ahead scheduling of IMGs, the uncertainties mainly come from the forecasting errors of RESs and load [31]. The required reserve capacities of IMG at time t caused by forecasting errors can be expressed as:

$$\begin{cases} R_t^+ = \max(e_{L,t} - e_{WT,t} - e_{PV,t}, 0) \\ R_t^- = \max(e_{WT,t} + e_{PV,t} - e_{L,t}, 0) \end{cases} \quad (1)$$

where R_t^+ and R_t^- are the required positive and negative reserve capacities of IMGs at time t , respectively; and $e_{WT,t}$, $e_{PV,t}$ and $e_{L,t}$ are the forecasting errors of WT, PV, and load at time t , respectively. The required positive reserve capacity indicates that there is a power shortage in the IMG, which needs to be addressed by upward regulation of power. On the contrary, the required negative reserve capacity indicates that the surplus power needs to be absorbed by using downward regulation of power.

The uncertainties of RESs are described by using scenario-based approaches, which can not only represent the probability distribution of forecasting power of PV and WT in time-power dimension, but also further reflect the correlation of these random variables. In this paper, scenario-based approaches are used to describe the forecasting errors of RESs and load. Assume that $R_{t,s}^+$ and $R_{t,s}^-$ represent the required positive and negative reserve capacities of IMG in scenario s at time t , respectively, according to (1), they can be expressed as:

$$\begin{cases} R_{t,s}^+ = \max(e_{L,t,s} - e_{WT,t,s} - e_{PV,t,s}, 0) \\ R_{t,s}^- = \max(e_{WT,t,s} + e_{PV,t,s} - e_{L,t,s}, 0) \end{cases} \quad (2)$$

where $e_{WT,t,s}$, $e_{PV,t,s}$, and $e_{L,t,s}$ are the forecasting errors of WT, PV, and load in scenario s at time t , respectively.

Assuming that the forecasting errors follow a certain prob-

ability distribution, multiple scenarios of forecasting error for IMGs can be constructed. When the positive and negative reserve capacities provided by IMGs in each scenario fail to meet the actual positive and negative reserve requirements, the lost load and RES power curtailment will occur, respectively. The mechanism is explained in Fig. 3.

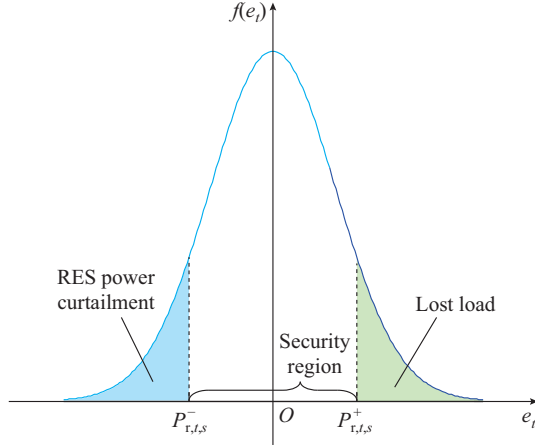


Fig. 3. Mechanism of lost load and RES power curtailment.

In Fig. 3, $f(e_t)$ is the probability distribution of forecasting error at time t for IMGs; and $P_{r,t,s}^+$ and $P_{r,t,s}^-$ are the provided positive and negative reserve capacities of IMGs, respectively. From Fig. 3, the positive error indicates that there is a power shortage in the IMG (i.e., the load is larger than the generation), thus the upward reserve capacity is required to balance the power shortage, which can be calculated by (2). If the actual provided reserve capacity $P_{r,t,s}^+$ is lower than $R_{t,s}^+$, the lost load will occur. Similarly, the negative error implies that there is power surplus in the IMG, thus the downward reserve capacity is required to absorb the surplus power. If $P_{r,t,s}^-$ is lower than $R_{t,s}^-$, the RES power curtailment will occur. Security region in Fig. 3 is an interval bounded by $P_{r,t,s}^+$ and $P_{r,t,s}^-$ within which the forecasting error can be accommodated by the system without causing operation risk.

As for the loss of lost load and RES power curtailment arising from the insufficient reserve, the loss function can be formulated as:

$$\begin{cases} C_{LL,t,s} = V_{VOLL} \max(R_{t,s}^+ - P_{r,t,s}^+, 0) \\ C_{RESC,t,s} = V_{RESC} \max(R_{t,s}^- - P_{r,t,s}^-, 0) \end{cases} \quad (3)$$

where $C_{LL,t,s}$ and $C_{RESC,t,s}$ are the losses of lost load and RES power curtailment, respectively; V_{VOLL} is the per unit loss value of lost load (VOLL); and V_{RESC} is the per unit loss value of RES power curtailment. In (3), the expressions of $P_{r,t,s}^+$ and $P_{r,t,s}^-$ are given as:

$$\begin{cases} P_{r,t,s}^+ = R_{gen,t,s}^+ + R_{ES,t,s}^+ + R_{IL,t,s}^+ \\ P_{r,t,s}^- = R_{gen,t,s}^- + R_{ES,t,s}^- \end{cases} \quad (4)$$

where $R_{gen,t,s}^+$ and $R_{gen,t,s}^-$ are the upward and downward reserve capacities provided by DPDGs, respectively; $R_{ES,t,s}^+$ and $R_{ES,t,s}^-$ are the provided upward and downward reserve capacities of ES, respectively; and $R_{IL,t,s}^+$ is the provided upward reserve capacity of IL.

Under a certain reserve decision, the high penetration of

RESs will increase the uncertainties of system operation, which is manifested by the amplitude expansion of the distribution of loss cost. It presents “fat tail” of the loss distribution, which leads to an inaccurate tail risk measure by VaR [26]. In order to effectively avoid the possible high loss caused by tail risk, CVaR is employed to measure the potential risk loss for IMG under a reserve decision.

According to the calculation method of discrete CVaR, the CVaR of lost load and RES power curtailment yielded by forecasting errors can be expressed as:

$$\begin{cases} C_{CVaR,t}^+ = C_{VaR,t}^+ + \frac{1}{1-\alpha^+} \sum_{s=1}^{\psi} \rho_s \max(C_{LL,t,s} - C_{VaR,t}^+, 0) \\ C_{CVaR,t}^- = C_{VaR,t}^- + \frac{1}{1-\alpha^-} \sum_{s=1}^{\psi} \rho_s \max(C_{RESC,t,s} - C_{VaR,t}^-, 0) \end{cases} \quad (5)$$

where $C_{VaR,t}^+$ and $C_{CVaR,t}^+$ are the VaR and CVaR of the lost load at a confidence level α^+ , respectively; $C_{VaR,t}^-$ and $C_{CVaR,t}^-$ are the VaR and CVaR of the RES power curtailment at a confidence level α^- , respectively; ψ is the number of scenarios; and ρ_s is the probability of scenario s .

According to (5), $C_{VaR,t}^+$ and $C_{CVaR,t}^+$ need to be calculated to solve (5). However, it is often difficult to solve $C_{VaR,t}^+$ and $C_{CVaR,t}^+$ directly according to its definition [25], [32]. An alternative approach is reported in [32], [35] by introducing auxiliary variable ζ and setting up a minimization problem for ζ to solve (5), which is expressed as:

$$\begin{cases} C_{CVaR,t}^+ = \min \zeta^+ + \frac{1}{(1-\alpha^+)} \sum_{s=1}^{\psi} \rho_s \max(C_{LL,t,s} - \zeta^+, 0) \\ C_{CVaR,t}^- = \min \zeta^- + \frac{1}{(1-\alpha^-)} \sum_{s=1}^{\psi} \rho_s \max(C_{RESC,t,s} - \zeta^-, 0) \end{cases} \quad (6)$$

where ζ^+ and ζ^- are the optimal values of VaR at confidence levels α^+ and α^- , respectively [32].

IV. LHS-BASED RANDOM SCENARIO GENERATION METHOD CONSIDERING CORRELATION

The key of discrete CVaR is to generate the random scenario of forecasting errors of RESs and load. Two types of methods are generally used for scenario generation of forecasting errors, which are MCS [12] and MCS followed by scenario reduction technique [31]. However, these methods have the following shortcomings. On the one hand, MCS relies on large-scale sampling, which inevitably faces the scenario dimension disaster. Furthermore, the combination explosion of control variables in the reserve optimization will aggravate the computational complexity. On the other hand, although MCS followed by scenario reduction technique [31] can reduce the scenario scale, the selection of typical scenarios cannot ensure that low-probability and high-risk scenarios are not cut off, which causes the risk leakage problem.

LHS is a special multi-dimensional stratified sampling method, which exhibits higher sampling efficiency than MCS [36]. Generally, LHS is mainly aimed at the case where random variables are independent of each other. Considering that IMGs belong to a small system, the power outputs of RESs have a strong correlation. Therefore, LHS-

based random scenario generation for forecasting errors should consider the correlation of input random variables.

LHS considering correlation mainly consists of the two steps: sampling and permutation.

1) Sampling

The core idea of sampling is to ensure that the probability distribution space of each input random variable can be covered by the sampling points completely. $\mathbf{X}=[X_1, X_2, \dots, X_n]$ denotes the n input random variables of the probabilistic problem to be solved, and the cumulative distribution function (CDF) of the k^{th} random variable is expressed as $F_k(X_k)$. According to the definition of CDF, $F_k(X_k)$ is a continuous monotone increasing function within $[0,1]$. With defined sample size N , the principle of sampling is as follows.

The scale of $F_k(X_k)$ is equally divided into N intervals, and the width of each interval is $1/N$. The median value of each interval is selected as the sampling point, then the value of the i^{th} sampling point of the k^{th} random variable X_{ki} can be calculated by:

$$X_{ki} = F_k^{-1}\left(\frac{i-0.5}{N}\right) \quad (7)$$

where F_k^{-1} is the inverse function of F_k .

2) Permutation

The purpose of permutation is to control the correlation of the samples of input variables, and make the correlation of the samples as close as possible to that of the actual input variables. The procedure for the transformation and permutation of the sampling points is as follows.

Step 1: assume that there are m correlated random variables and the correlation coefficient matrix is \mathbf{R}_X .

Step 2: based on the CDF of input random variables and their correlation coefficient matrix \mathbf{R}_X , the correlation matrix \mathbf{R}_Y of the m -dimension correlated sample matrix \mathbf{Y} with standard normal distribution can be obtained. The process can be found in [37].

Step 3: with sample size N , the m -dimension independent sample matrix \mathbf{Z} with standard normal distribution can be obtained according to LHS mentioned in (1). Thus, \mathbf{Z} is an $m \times N$ sample matrix.

Step 4: apply Cholesky decomposition to \mathbf{R}_Y to obtain the lower triangular matrix \mathbf{B}_Y , and then calculate \mathbf{Y} by $\mathbf{Y} = \mathbf{B}_Y \mathbf{Z}$.

Step 5: obtain the ordering matrix \mathbf{L}_S from \mathbf{Y} .

Step 6: sample the input random variables \mathbf{X} using the LHS method to generate the $m \times N$ sample matrix \mathbf{W} according to their respective probability distribution models. The final correlated sample matrix \mathbf{S} is obtained by permuting the samples according to the ordering matrix \mathbf{L}_S .

V. MODELING OF JOINT ENERGY AND RESERVE SCHEDULING FOR IMGs

The day-ahead scheduling of IMGs should focus on the following two objective requirements: ① it is required to realize the optimal economic scheduling of IMGs on the premise of satisfying the power balance between generation and load; ② it is necessary to consider the operation risk and reserve requirement caused by the forecasting errors of RESs and load, so as to provide a decision-making reference for

actual operation scheduling.

As for the first requirement, a day-ahead optimal economic scheduling model for IMG is developed with the objective function of the total scheduling cost, then the power balance constraint and the operation constraint of each schedulable unit are put into the constraints of the model. As for the second requirement, the CVaR theory is employed for risk-based reserve decision, which is placed in the objective function to control the operation risk in the optimization process.

A. Objective Function

Based on the analysis above, the objective of the joint energy and reserve scheduling is to minimize the total scheduling cost and CVaR, which is expressed as:

$$\min C = C_{\text{dis}} + \beta C_{\text{CVaR}} \quad (8)$$

where C_{dis} is the total scheduling cost of IMG; C_{CVaR} is the CVaR of IMG operation; and β is the risk-aversion coefficient, and the value can be set according to the risk preference of decision-makers. If the operation and maintenance cost of RESs is ignored, the generation cost of RESs can be regarded as 0. Thus, C_{dis} and C_{CVaR} can be expressed as:

$$C_{\text{dis}} = \sum_{t=1}^T \sum_{s=1}^S \rho_s (C_{\text{gen},t,s} + C_{\text{ES},t,s} + C_{\text{IL},t,s} + C_{\text{gen},t,s}^r + C_{\text{ES},t,s}^r + C_{\text{IL},t,s}^r + C_{\text{LL},t,s} + C_{\text{RESC},t,s}) \quad (9)$$

$$C_{\text{CVaR}} = \sum_{t=1}^T (C_{\text{CVaR},t}^+ + C_{\text{CVaR},t}^-) \quad (10)$$

where $C_{\text{gen},t,s}$, $C_{\text{ES},t,s}$, and $C_{\text{IL},t,s}$ are the generation cost of DP-DG, the operation cost of ES, and the operation cost of IL, respectively; $C_{\text{gen},t,s}^r$, $C_{\text{ES},t,s}^r$, $C_{\text{IL},t,s}^r$ are the reserve costs paid by IMG to the DP-DG, ES and IL, respectively; and T is the number of time periods for a scheduling period.

In this paper, the energy cost generated by the actual invoked reserve in operation is not considered, and the reserve cost is only related to the provided reserve capacity. Each cost is calculated by:

$$\begin{cases} C_{\text{gen},t,s} = \sum_{i=1}^{N_G} (a_{\text{gen},i} P_{\text{gen},i,t,s}^2 + b_{\text{gen},i} P_{\text{gen},i,t,s} + S_{\text{gen},i,t,s}^{\text{on}}) \\ C_{\text{ES},t,s} = a_{\text{ES}} |P_{\text{ES},t,s}| \\ C_{\text{IL},t,s} = a_{\text{IL}} P_{\text{IL},t,s} \end{cases} \quad (11)$$

$$\begin{cases} C_{\text{gen},t,s}^r = \sum_{i=1}^{N_G} (c_{\text{gen},i}^+ R_{\text{gen},i,t,s}^+ + c_{\text{gen},i}^- R_{\text{gen},i,t,s}^-) \\ C_{\text{ES},t,s}^r = c_{\text{ES}}^+ R_{\text{ES},t,s}^+ + c_{\text{ES}}^- R_{\text{ES},t,s}^- \\ C_{\text{IL},t,s}^r = c_{\text{IL}}^+ R_{\text{IL},t,s}^+ \end{cases} \quad (12)$$

where N_G is the number of DP-DGs in IMG; $P_{\text{gen},i,t,s}$, $P_{\text{ES},t,s}$, and $P_{\text{IL},t,s}$ are the generated power of DP-DG i , the power of ES, and the shedding power of IL, respectively, and $P_{\text{ES},t,s}$ can be positive or negative, which indicates that ES is charging or discharging, respectively; $a_{\text{gen},i}$ and $b_{\text{gen},i}$ are the cost coefficients of the cost function of DP-DG i ; $S_{\text{gen},i,t,s}^{\text{on}}$ is the start-up cost of DP-DG i ; a_{ES} and a_{IL} are the operation costs for per unit power of ES and IL, respectively; $R_{\text{gen},i,t,s}^+$ and $R_{\text{gen},i,t,s}^-$ are the provided upward and downward reserve capacities of DP-DG i , respectively; $c_{\text{gen},i}^+$ and $c_{\text{gen},i}^-$ are the upward

and downward reserve costs for per unit capacity of DPDG i , respectively; c_{ES}^+ and c_{ES}^- are the upward and downward reserve costs for per unit capacity of ES, respectively; and c_{IL}^+ is the upward reserve cost for per unit capacity of IL.

B. Constraints

The proposed objective function is subject to the following constraints.

1) Power balance constraint of IMG. Power supplied from schedulable units and RESs must satisfy the load demand in an IMG.

$$\sum_{i=1}^{N_G} P_{gen,i,t,s} + P_{WT,t,s} + P_{PV,t,s} - P_{RES,t,s}^{curt} - P_{ES,t,s} = P_{L,t,s} - P_{IL,t,s} \quad (13)$$

where $P_{WT,t,s}$ and $P_{PV,t,s}$ are the power outputs of WT and PV, respectively; $P_{L,t,s}$ is the total load of IMG; and $P_{RES,t,s}^{curt}$ is the power curtailment of RES, which can be expressed as:

$$\begin{cases} P_{RES,t,s}^{curt} = \max(R_{t,s}^+ - P_{t,s}^-, 0) \\ P_{RES,t,s}^{curt} \leq P_{WT,t,s} + P_{PV,t,s} \end{cases} \quad (14)$$

2) Operation constraints for DPDGs. Constraints (15) and (16) limit the power of DPDGs and the ramping rate, respectively. Constraint (17) identifies the start-up cost of DPDGs. Constraint (18) ensures the minimum on and off durations for DPDGs.

$$u_{gen,i,t,s} P_{gen,i}^{\min} \leq P_{gen,i,t,s} \leq u_{gen,i,t,s} P_{gen,i}^{\max} \quad (15)$$

$$-r_{d,i} \Delta t \leq P_{gen,i,t,s} - P_{gen,i,t-1,s} \leq r_{u,i} \Delta t \quad (16)$$

$$\begin{cases} S_{gen,i,t,s}^{\text{on}} \geq c_{gen,i}^{\text{on}} (u_{gen,i,t,s} - u_{gen,i,t-1,s}) \\ S_{gen,i,t,s}^{\text{on}} \geq 0 \end{cases} \quad (17)$$

$$\begin{cases} (u_{gen,i,t,s} - u_{gen,i,t-1,s}) T_{gen,i}^{\text{on}} + \sum_{j=t-T_{gen,i}^{\text{on}}}^{t-1} u_{gen,i,j,s} \geq 0 \\ (u_{gen,i,t-1,s} - u_{gen,i,t,s}) T_{gen,i}^{\text{off}} + \sum_{j=t-T_{gen,i}^{\text{off}}}^{t-1} (1 - u_{gen,i,j,s}) \geq 0 \end{cases} \quad (18)$$

where $u_{gen,i,t,s}$ is a state variable of DPDG i (1 indicates that the unit is on and 0 otherwise); $r_{u,i}$ and $r_{d,i}$ are the upward and downward ramping rates of DPDG i , respectively; Δt is the time interval, which is set to be 1 hour in this paper; $c_{gen,i}^{\text{on}}$ is the per unit start-up cost of DPDG i ; $T_{gen,i}^{\text{on}}$ and $T_{gen,i}^{\text{off}}$ are the minimum on and off durations, respectively; and $P_{gen,i}^{\min}$ and $P_{gen,i}^{\max}$ are the lower and upper power limits of DPDG i in operation, respectively. Generally, $P_{gen,i}^{\max}$ equals to the rated capacity, and $P_{gen,i}^{\min}$ is the minimum allowable output, which equals to $\gamma P_{gen,i}^{\max}$ and γ is usually set to be 30%-40% for MTs or diesel generators.

The reserve scheduling of DPDGs is limited by reserve response time, which is defined as τ , thus the reserve capacity constraints of DPDGs are as follows.

$$\begin{cases} 0 \leq R_{gen,i,t,s}^+ \leq \min(u_{gen,i,t,s} r_{u,i} \tau, u_{gen,i,t,s} P_{gen,i}^{\max} - P_{gen,i,t,s}) \\ 0 \leq R_{gen,i,t,s}^- \leq \min(u_{gen,i,t,s} r_{d,i} \tau, P_{gen,i,t,s} - u_{gen,i,t,s} P_{gen,i}^{\min}) \end{cases} \quad (19)$$

3) Operation constraints for ES. State of charge (SOC) reveals the energy balance of ES and reflects the dynamic behaviour of ES. Constraint (20) forms the SOC constraint, and it also guarantees SOC balance of ES during the sched-

uling period and ensures the SOC within the minimum/maximum SOC. Constraint (21) is the power constraint of ES which aims to limit the charging/discharging power and reserve capacity.

$$\begin{cases} S_{ES,t,s} = S_{ES,t-1,s} + \left(\frac{u_{t,s}^c P_{ES,t,s} \eta_c}{E_{ES}} + \frac{u_{t,s}^d P_{ES,t,s}}{\eta_d E_{ES}} \right) \Delta t \\ S_{ES,T,s} = S_{ES,0,s} \\ S_{ES}^{\min} \leq S_{ES,t,s} \leq S_{ES}^{\max} \\ u_{t,s}^c + u_{t,s}^d \leq 1 \end{cases} \quad (20)$$

$$\begin{cases} P_{ES,t,s} + R_{ES,t,s}^- \leq \min \left(P_{ES}, \frac{(S_{ES}^{\max} - S_{ES,t,s}) E_{ES}}{\eta_c \Delta t} \right) \\ P_{ES,t,s} - R_{ES,t,s}^+ \geq \max \left(-P_{ES}, \frac{(S_{ES}^{\min} - S_{ES,t,s}) E_{ES}}{\Delta t} \eta_d \right) \\ R_{ES,t,s}^+ \geq 0 \\ R_{ES,t,s}^- \geq 0 \end{cases} \quad (21)$$

where E_{ES} is the rated capacity of ES; $S_{ES,t,s}$ is the SOC of ES; S_{ES}^{\min} and S_{ES}^{\max} are the lower and upper SOC limits of ES, respectively; $u_{t,s}^c$ is a binary variable, which equals 1 if ES is charging and 0 otherwise; $u_{t,s}^d$ is a binary variable, which equals 1 if ES is discharging and 0 otherwise; η_c and η_d are the charging and discharging efficiencies of ES, respectively; $S_{ES,0,s}$ and $S_{ES,T,s}$ are the initial and final SOC of ES during the scheduling period, respectively; and P_{ES} is the rated power of ES.

4) Operation constraints for IL. The power and reserve capacity of IL are limited in (22).

$$\begin{cases} 0 \leq P_{IL,t,s} + R_{IL,t,s}^+ \leq P_{IL,t,s}^{\max} \\ P_{IL,t,s} \geq 0 \\ R_{IL,t,s}^+ \geq 0 \end{cases} \quad (22)$$

where $P_{IL,t,s}^{\max}$ is the upper power limit of IL, which equals the IL of IMG.

C. Solution Methodology

The discrete CVaR is introduced and employed to measure the potential loss caused by operation risk. Meanwhile, the LHS considering correlation is adopted to generate the random scenarios of forecasting errors for RESs and load. The optimization model of day-ahead scheduling for IMGs considering CVaR, includes the following decision variables: the generated power and on/off state variables of DPDGs, the charging/discharging power of ES, the shedding power of IL, and the reserve decision variables of generation, load, and storage, etc.

As the objective function is a quadratic function and the constraints contain binary decision variables, the model is a mixed-integer nonlinear programming problem. The method of piecewise linearization [22], [38], [39] is applied to linearize the quadratic function in the model. Due to the space limitation, the linearization process will not be repeated. After the linearization, the mixed-integer linear programming model is solved by CPLEX solver called from YALMIP in MATLAB environment.

VI. CASE STUDIES

A. Input Data

The typical IMG shown in Fig. 1 is used as the simulation system. MT is taken as the DPDG, which provides the power supply and reserve support.

The economic parameters and technical parameters of MT, ES and IL are shown in Appendix A Table AI. The maximum day-ahead forecasting load of IMG is 160 kW. The installed capacity of MT is 150 kW. The maximum day-ahead forecasting power outputs of WT and PV are 50 kW and 30 kW, respectively. The sum of the maximum forecasting power of WT and PV accounts for 50% of the maximum load, which reflects the scenario with high penetration of RESs. The maximum power and rated capacity of battery ES system are 15 kW and 75 kWh, respectively. V_{VOLL} and V_{RESC} are set to be 1 \$/kWh and 0.2 \$/kWh, respectively. The confidence level α is generally chosen between 0.9 and 0.99 in day-ahead scheduling of MGs [30]. According to [22], [31], the confidence level of CVaR is set as $\alpha^+ = \alpha^- = 0.95$. Assume that decision-makers begin to focus on operation risk but still have a certain risk tolerance, the risk-aversion coefficient β can be set to be 1. That is, decision-makers attach equal importance to CVaR and the total scheduling cost. The scheduling period is set to be 1 day (24 hours), thus $T=24$.

The day-ahead forecasting power of WT, PV, and load is given in Appendix A Fig. A1, and the per-unit value is adopted to show the peak-valley relationship clearly. As shown in Appendix A Fig. A1, it presents the inverse peak-valley characteristic between WT and load, and the complementary between WT and PV.

Normal distribution is widely used to model the uncertainties of forecasting errors [12]–[15]. In this case, the standard deviation of the day-ahead forecasting error of load is assumed to be 10% of its mean value, and the standard deviations of power forecasting errors for WT and PV are set to be 20% of their mean values. According to Section IV, the forecasting errors of WT, PV, and load in an IMG are often correlated.

Considering the complementarity of WT-PV, the correlation coefficient is negative and is set to be $\rho_{\text{WT,PV}} = -0.3$. According to the strong inverse peak-valley characteristics between WT and load, the correlation coefficient is negative and is set to be $\rho_{\text{WT,L}} = -0.5$. Similarly, the correlation coefficient between PV and load is set to be $\rho_{\text{PV,L}} = 0.2$. Consequently, the correlation coefficient matrix can be formulated

$$\text{as } \mathbf{R}_{\text{WT,PV,L}} = \begin{bmatrix} 1.0 & -0.3 & -0.5 \\ -0.3 & 1.0 & 0.2 \\ -0.5 & 0.2 & 1.0 \end{bmatrix}.$$

B. Verification of LHS Considering Correlation

MCS is the most popular method for random scenario generation, which relies on a large-scale sampling and is commonly used as a benchmark to verify the accuracy of other methods [16]. In order to break through the huge computational burden brought by MCS, MCS combined with clustering algorithm is widely used for scenario reduction [31]. To highlight the accuracy and superiority of the proposed LHS-

based random scenario generation method, it is compared with the two popular methods above. The day-ahead forecasting power of WT, PV, and load in time period 10 (WT: 22 kW, PV: 15.9 kW, load: 130 kW) is selected as the mean value, and the following three comparative schemes are designed.

Scheme 1: MCS (benchmark). MCS considering the correlation of random variables is performed with the sample size of 10000.

Scheme 2: MCS + scenario reduction. Based on the samples generated by scheme 1, fuzzy c -means algorithm [40], [41] is used to achieve scenario reduction, and then 500 samples of WT, PV, and load forecasting power are obtained.

Scheme 3: LHS considering correlation. The proposed LHS-based scenario generation method considering correlation is utilized to obtain the forecasting power. The sample size is 500, which is the same as scheme 2.

Table I lists the detailed numerical results of the mean value and the standard deviation of the three schemes.

TABLE I
COMPARISON OF MEAN VALUE AND STANDARD DEVIATION

Unit	Mean value (kW)			Standard deviation (kW)		
	1	2	3	1	2	3
WT	22.00	21.95	22.00	4.387	19.619	4.394
PV	15.90	15.90	15.90	3.170	14.177	3.176
Load	130.01	130.00	130.00	12.961	57.964	12.983

The results in Table I are analyzed as follows.

1) The mean values of the three schemes are very close, which are highly approximate to the forecasting power of WT, PV and load in time period 10. It means that the three schemes can obtain relatively uniform and accurate mean values of samples.

2) In terms of standard deviation, the standard deviation of scheme 3 is very close to scheme 1, with an error of less than 0.2%. The standard deviations of schemes 1 and 3 are consistent with the preset standard deviations (load: 10% of the mean value; WT and PV: 20% of the mean value), and the standard deviation of scheme 3 is closer to the preset standard deviation than scheme 1, which fully demonstrates the accuracy of scheme 3.

3) As the scenario reduction in scheme 2 sacrifices the probability information and accuracy of samples to some extent, the difference between the standard deviation of scheme 2 and the preset standard deviation is relatively large.

Therefore, it reveals that LHS can provide accurate approximation to the forecasting power with smaller sample size, which reflects its superior sampling efficiency. Compared with scheme 2, the probability information of samples obtained by LHS is closer to the preset standard distribution of random variables.

In order to examine the correlation level of samples generated by scheme 3, the power samples in each time period are counted to calculate their correlation coefficients, which are shown in Fig. 4. The solid lines in Fig. 4 represent the preset correlation coefficients, and the scatter points repre-

sent the actual correlation coefficients. All scatter points are located near the solid lines, which indicates that the correlation coefficients of power samples obtained by scheme 3 in each time period can follow the preset correlation coefficients.

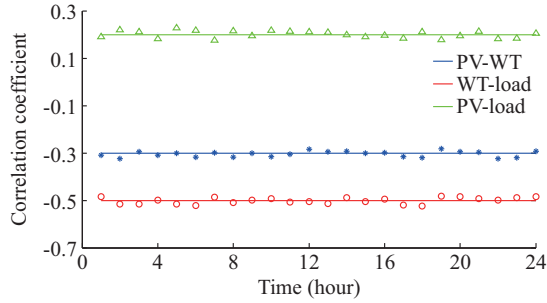


Fig. 4. Correlation coefficients of power samples in each time period.

C. Analysis of Operation Results

Based on the sample data of scheme 3, the forecasting power samples of WT, PV, and load with sample size of 500 are formed. Based on the proposed model, the cost indices of optimization results are calculated, which are as follows: the operation cost of IMG is \$208.07, the reserve cost is \$14.18, the expected loss of lost load and RES power curtailment is \$2.73, the total dispatching cost is \$224.98, and the CVaR is \$47.73. It can be seen that the proposed model can greatly reduce the loss of lost load and RES power curtailment, which is beneficial to improving the economy and reliability of IMG.

In order to further investigate the power balance of IMG and the output of each schedulable unit, an expected scenario is chosen, and the power histogram of each schedulable unit is given in Fig. 5. In Fig. 5, the output power is defined as positive. Thus, the charging power of ES and the curtailed power of RES (opposite to the generated power of RES) can be denoted as negative.

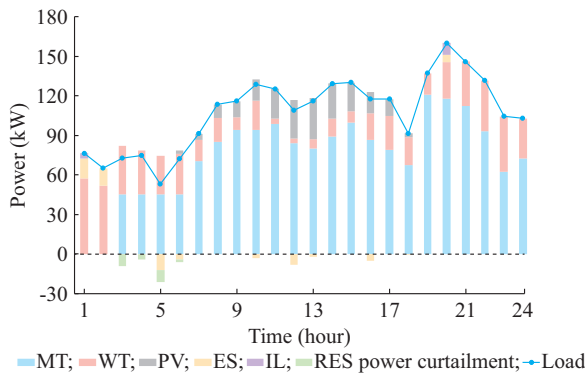


Fig. 5. Power of each schedulable unit in expected scenario.

As shown in Fig. 5, the load of each time period is equal to the sum of the power of each schedulable unit and RES, thus the IMG can maintain power balance. In the peak load period (period 20), as a certain positive reserve capacity is allocated to cope with the forecasting errors, the power output of MT and ES cannot balance the actual load demand, consequently, thus the load shedding occurs. As for the peri-

od when the MT is on and the WT output is relatively high, due to the limitation of the minimum operation power of the MT, RES power curtailment is adopted to balance the power. The ES is charged when the PV output is surplus or the load is low, and is discharged during the peak load period or when the MT is off, which conforms to the scheduling rules. Therefore, the proposed day-ahead scheduling model for IMGs is reasonable and effective.

To evaluate the effect of confidence levels α^+ and α^- on CVaR, the discussion and analysis of CVaR with different values of α^+ and α^- (from 0.50 to 0.99) on the premise of $\alpha^+ = \alpha^- = \alpha$ are given in Fig. 6. CVaR reveals the occurrence probability of risk, which is $1 - \alpha^+$ or $1 - \alpha^-$, and provides an intuitive reference to system security. The confidence level of risk-based reserve decision increases as α^+ and α^- go up, which indicates the increased risk aversion of decision-makers, and thus the more extreme situation in the loss distribution tend to be chosen as a decision reference to measure the potential risk loss of IMG. Hence, in the case of high confidence level (where high security is required), CVaR (risk cost) will increase.

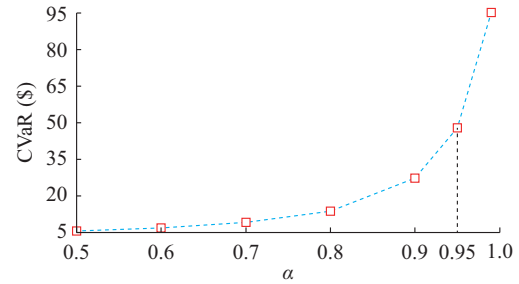


Fig. 6. Relationship between CVaR and confidence level.

According to the objective function in (8), different risk-aversion coefficients reflect the different attitudes of decision-makers towards the risk. The values of β are set to be 3.0, 2.5, 2.0, 1.5, 1.0, 0.5, and the Pareto front is shown in Fig. 7.

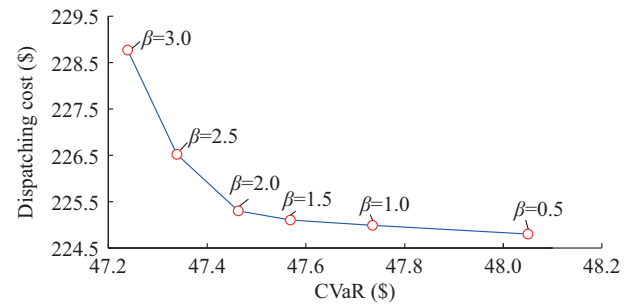


Fig. 7. Pareto front of different risk-aversion coefficients.

With the rise of β , the total scheduling cost of IMG increases gradually, whereas the corresponding CVaR decreases monotonically. When $\beta = 0.5$, as the lack of enough attention to risk, the scheduling mainly focuses on the operation economy of IMG, which leads to a low reserve capacity allocation in reserve decision. On the one hand, although the total dispatching cost can be reduced for the smaller value of

β , the CVaR representing the potential loss resulting from insufficient reserve is relatively high. On the other hand, for the higher value of β , decision-makers tend to pay more attention to the loss caused by forecasting errors, which sacrifices the economy of scheduling to some extent.

D. Analysis on Generation-load-storage Multi-type Reserve Scheme

In order to evaluate the impact of the proposed generation-load-storage multi-type reserve scheme on IMG operation, four reserve schemes are designed for comparative analysis. The specific schemes are shown in Table II. Through optimization calculation, the daily operation cost indices of IMG in the four reserve schemes are listed in Table III.

TABLE II
DESIGN OF DIFFERENT RESERVE SCHEMES

Scheme	MT	IL	ES
1	+	−	−
2	+	+	−
3	+	−	+
4	+	+	+

Note: “+” and “−” represent with and without participation in provision of reserve, respectively.

TABLE III
COMPARISON OF OPERATION COST INDICES OF IMG IN DIFFERENT RESERVE SCHEMES

Scheme	Total scheduling cost C_{dis} (\$)	Loss of lost load and RES power curtailment (\$)	Reserve cost (\$)	CVaR (\$)
1	255.76	30.19	7.57	402.08
2	240.83	16.35	9.53	168.94
3	230.18	5.52	11.23	65.66
4	224.98	2.73	14.18	47.73

Scheme 1 merely utilizes DPDGs to provide single spinning reserve support for IMG [10], [19], which is the main reserve scheme of traditional power grid. Scheme 2 adds IL as demand response resources to support the reserve shortage during the peak load period [31], [32], and the loss of lost load is greatly reduced. In scheme 3, ES is added to participate in providing upward/downward reserve capacity. Compared with scheme 1, the loss of lost load and RES power curtailment decreases by 81.7%. Scheme 4 is the proposed generation-load-storage multi-type reserve scheme. ES combined with IL can further mitigate the shortage of upward/downward reserve capacity, so that the expected loss of lost load and RES power curtailment is the minimum.

Although scheme 4 increases the reserve cost to some extent, compared with schemes 1 and 2, the total dispatching cost is reduced by 12% and 6.6%, respectively. It indicates that scheme 4 not only improves the economy and reliability of IMG, but also effectively promotes the RES accommodation. Meanwhile, the CVaR of scheme 4 is the minimum, which decreases sharply by 88% and 72%, respectively, compared with those of schemes 1 and 2. The results demonstrate that scheme 4 can significantly reduce the potential

risk of lost load and RES power curtailment, and meet the requirement of reserve capacity for high-risk aversion.

E. Effect of Correlation on IMG Operation

In order to evaluate the influence of the correlation of forecasting errors on system operation, different correlation coefficients are designed for comparative analysis.

Case 1: the correlation coefficients among forecasting errors are not considered, namely, the correlation coefficient

$$\text{matrix is } \mathbf{R}_{WT,PV,L} = \begin{bmatrix} 1 & 0 & 0 \\ 0 & 1 & 0 \\ 0 & 0 & 1 \end{bmatrix}.$$

Case 2: the correlation coefficient matrix is set to be

$$\mathbf{R}_{WT,PV,L} = \begin{bmatrix} 1 & 0.3 & 0.5 \\ 0.3 & 1 & -0.2 \\ 0.5 & -0.2 & 1 \end{bmatrix}, \text{ which is inverse to Section VI-A.}$$

Case 3: the correlation coefficient matrix is set to be the same with that in Section VI-A

According to the correlation coefficient matrices set in the three cases, LHS considering correlation is used to obtain the sample data of each time period of RES and load. The independent optimization is performed based on the proposed optimal day-ahead scheduling model to obtain the cost indices, which are shown in Table IV.

TABLE IV
COMPARISON OF COST INDICES IN DIFFERENT CASES

Case	Total dispatching cost (\$)	Reserve cost (\$)	CVaR (\$)
1	221.99	12.88	32.46
2	217.03	9.99	15.24
3	224.98	14.18	47.73

In the three cases, the cost indices are different from each other. Hence, it is necessary to consider the correlation of forecasting errors, which can make the scheduling results more reasonable. The three cost indices of case 3 are the largest. It can be explained as follows.

1) As the absolute value of the negative correlation coefficient between WT and load in case 3 is high (strong correlation), i.e., $\rho_{WT,L} = -0.5$, in the scenario where the forecasting error of load e_L is positive (the load demand is underestimated), the forecasting error of WT e_W has a greater probability to be negative (the power output of WT is overestimated). Similarly, when e_L is negative, e_W has a higher probability to be positive. It leads to a result that, compared with case 1, case 3 requires larger positive/negative reserve capacity to maintain the power balance of IMG to avoid the occurrence of lost load or the RES power curtailment. Moreover, due to the limitation of actual reserve capacity, the expected loss of lost load and RES power curtailment in case 3 is higher than that of case 1, which results in the total dispatching cost and CVaR are also higher.

2) There is a negative correlation coefficient between WT and PV (complementarity), and a positive correlation coefficient between PV and load (can alleviate the negative effect of e_L on IMG to some extent). Nonetheless, the peak power of load and WT occurs in the evening when PV output is 0.

Therefore, the impact on operation indices is not as obvious as the inverse peak-valley characteristics of WT and load.

3) Case 2 is the inverse correlation case of case 3, thus the three cost indices are the smallest among the three cases.

F. Analysis on Different Integrated Capacities of RES

The capacity of RES in Section VI-A is taken as the basis capacity. Then, different integrated capacities of RES are set as 0.8 basis capacity, basis capacity, 1.2 basis capacity, and 1.5 basis capacity. For different integrated capacities of RES, the calculation results of objective function of schemes 1 and 4 are given in Table V.

TABLE V
CALCULATION RESULTS OF SCHEMES 1 AND 4 WITH DIFFERENT
INTEGRATED CAPACITIES OF RES

Multiples of basis capacity	Capacity of RES (kW)		Scheme 1		Scheme 4	
	WT	PV	C_{dis} (\$)	CVaR (\$)	C_{dis} (\$)	CVaR (\$)
0.8	40	24	266.43	321.14	241.20	33.99
1.0	50	30	255.76	402.08	224.98	47.73
1.2	60	36	245.93	428.79	209.46	65.78
1.5	75	45	237.62	488.99	188.13	95.13

Since the generation cost of RES is approximately considered to be zero, the increase of RES penetration is beneficial to reducing the total dispatching cost of IMG. It implies that increasing the integrated capacity of RES plays a prominent role in improving the operation economy. In schemes 1 and 4, as the integrated capacity of RES increases, the increase of the forecasting error will lead to the rise of CVaR.

From the analysis of the difference of the total scheduling cost between scheme 1 and scheme 4, an increasing trend of the difference can be observed as the integrated capacity of RES increases. The reason is that the reserve shortage caused by the high penetration of RESs will result in a sharp rise in the expected loss of lost load and RES power curtailment if scheme 1 is used only. Compared with the basis capacity, in the situations of 1.2 and 1.5 basis capacity, the difference of the total dispatching cost between the two reserve schemes increases by 18.5% and 60.8%, respectively. The monotonous increase of the difference between the two schemes demonstrates that scheme 4 is more economical in the scenario of high penetration of RESs.

Approximately, with the increase of the integrated capacity of RES, the difference of CVaR between the two schemes also presents an expanding trend. It means that scheme 4 is more conducive to reducing the operation risk and improving the accommodation of RES for IMGs with high penetration of RESs.

G. Discussion on Applicability for Grid-connected MGs

As mentioned in Section I, the operation of IMGs is more sensitive to uncertainties compared with grid-connected MGs. Therefore, IMGs are taken as the research object in this paper. Nevertheless, the core contributions and methods of this paper are still applicable to grid-connected MGs. The explanation and discussion are as follows.

1) For grid-connected MGs, the main grid can provide up-

ward/downward reserve capacity and participate in reserve optimization. In other words, the proposed multi-type reserve scheme should consider the reserve resources on grid side as well. Based on the proposed multi-type reserve scheme, a new generation-grid-load-storage multi-type reserve scheme can also be built. Hence, (4) can be revised as:

$$\begin{cases} P_{t,l,s}^+ = R_{gen,t,s}^+ + R_{ES,t,s}^+ + R_{IL,t,s}^+ + R_{grid,t,s}^+ \\ P_{t,l,s}^- = R_{gen,t,s}^- + R_{ES,t,s}^- + R_{grid,t,s}^- \end{cases} \quad (23)$$

where $R_{grid,t,s}^+$ and $R_{grid,t,s}^-$ are the provided upward and downward reserve capacities of the main grid, respectively. Therefore, the proposed multi-type reserve scheme is still suitable for grid-connected MGs by introducing $R_{grid,t,s}^+$ and $R_{grid,t,s}^-$ to represent the reserve capacity from the main grid.

2) The sources of uncertainties for grid-connected MGs include not only the power forecasting errors of RESs and load, but also the electricity price [30], [42]. On the one hand, the forecasting error of electricity price is usually described by normal distribution [27], [31], and the electricity price can be considered to be correlated with the load demand [30], thus the proposed modeling of forecasting error considering correlation is also applicable to the modeling of electricity price. On the other hand, with regard to LHS-based random scenario generation method, we only need to add a random variable of electricity price to the input random variable and revise the correlation coefficient matrix \mathbf{R}_x according to Section IV. Hence, the proposed LHS-based random scenario generation scheme can also be applied to grid-connected MGs.

3) In order to match the operation characteristic of grid-connected MGs, the proposed model of joint energy and reserve scheduling considering risk-based reserve decision can be modified as follows. ① The loss functions $C_{LL,t,s}$ and $C_{RESC,t,s}$ in (6) are adopted to express the potential loss of lost load and RES power curtailment. But for grid-connected MGs, the loss function should be rewritten according to the specific risk measurement such as expected profit of MG [30], expected cost of MG [42], [43]. ② As grid-connected MGs may have power exchange with the main grid and purchase reserve capacity from it, the total scheduling cost C_{dis} in (8) should also include the cost/revenue of/from the power exchange with the main grid [42], and the reserve cost paid to the main grid [43]. Without loss of generality, through the above modification of the model, the proposed model of joint energy and reserve scheduling is still applicable to the co-optimization of energy and reserve for grid-connected MGs.

VII. CONCLUSION

In this paper, a generation-load-storage multi-type reserve scheme is proposed to solve the operation risk caused by the forecasting errors of RES and load. CVaR is introduced and employed for risk measurement of reserve decision, and an optimal day-ahead scheduling model of IMG is established. The conclusions are as follows.

1) The proposed multi-type reserve scheme can satisfy the flexibility requirements of high penetration of RES, and alleviate the shortage of the flexibility regulation capacity via single spinning reserve provided by DPDGs.

2) Comparisons with the conventional methods of MCS and MCS + scenario reduction show the effectiveness and superiority of the proposed LHS-based scenario generation method considering correlation as far as sample scale and accuracy are concerned. Furthermore, the correlation level of obtained power samples can follow the preset correlation coefficient.

3) The proposed model of joint energy and reserve scheduling considering risk-based reserve decision is evaluated by comprehensive case studies. The simulation results demonstrate that it is very necessary to consider the correlation of forecasting errors in the day-ahead scheduling, and the proposed model can satisfy different risk preferences of decision-makers and realize coordinated optimization of energy and reserve.

4) With the high penetration of RESs in IMG, the proposed multi-type reserve scheme can effectively improve the economy and reliability of IMG, and reduce the risk such as the occurrence of lost load and RES power curtailment, which is conducive to promoting the accommodation of high penetration of RESs for IMGs.

APPENDIX A

TABLE AI
ECONOMICAL AND TECHNICAL PARAMETERS OF MT, ES, AND IL

Parameter	Value	Parameter	Value
$a_{\text{gen},i}$	0.00015 \$/kW ²	$r_{u,i}, r_{d,i}$	90 kW/h
$b_{\text{gen},i}$	0.1 \$/kW	$P_{\text{gen},i}^{\min}$	45 kW
$c_{\text{gen},i}^{\text{on}}$	1.5 \$	$P_{\text{gen},i}^{\max}$	150 kW
a_{ES}	0.1 \$/kW	$T_{\text{gen},i}^{\text{on}}$	3 hours
a_{IL}	0.4 \$/kW	$T_{\text{gen},i}^{\text{off}}$	2 hours
$C_{\text{gen},i}^+, C_{\text{gen},i}^-$	0.035 \$/kW	η_c, η_d	0.9
$C_{\text{ES}}^+, C_{\text{ES}}^-$	0.035 \$/kW	S_{ES}^{\max}	0.9
C_{IL}^+	0.07 \$/kW	S_{ES}^{\min}	0.1

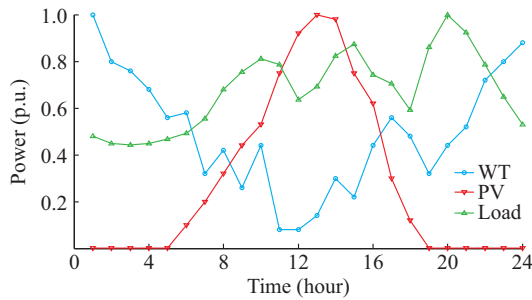


Fig. A1. Day-ahead forecasting power of WT, PV, and load.

REFERENCES

- [1] BP. BP energy outlook: 2019 edition. [Online]. Available: <https://www.bp.com/en/global/corporate/news-and-insights/press-releases/bp-energy-outlook-2019.html>
- [2] NDRC. Chinese energy production and consumption revolution strategy (2016-2030). [Online]. Available: http://www.gov.cn/xinwen/2017-04/25/content_5230568.htm
- [3] Y. Chen, W. Wei, F. Liu *et al.*, "Energy trading and market equilibrium in integrated heat-power distribution systems," *IEEE Transactions on Smart Grid*, vol. 10, no. 4, pp. 4080-4094, Jul. 2019.
- [4] F. R. Badal, P. Das, S. K. Sarker *et al.*, "A survey on control issues in renewable energy integration and microgrid," *Protection and Control of Modern Power Systems*, vol. 4, no. 1, pp. 1-27, Jan. 2019.
- [5] K. Lai, Y. Wang, D. Shi *et al.*, "Sizing battery storage for islanded microgrid systems to enhance robustness against attacks on energy sources," *Journal of Modern Power Systems and Clean Energy*, vol. 7, no. 5, pp. 1177-1188, Sept. 2019.
- [6] E. Shahryari, H. Shayeghi, B. Mohammadi-Ivatloo *et al.*, "A copula-based method to consider uncertainties for multi-objective energy management of microgrid in presence of demand response," *Energy*, vol. 175, pp. 879-890, Mar. 2019.
- [7] Z. Liu, Y. Yi, J. Yang *et al.*, "Optimal planning and operation of dispatchable active power resources for islanded multi-microgrids under decentralised collaborative dispatch framework," *IET Generation, Transmission & Distribution*, vol. 14, no. 3, pp. 408-422, Feb. 2020.
- [8] Y. Kuang, Y. Zhang, B. Zhou *et al.*, "A review of renewable energy utilization in islands," *Renewable and Sustainable Energy Reviews*, vol. 59, pp. 504-513, Jun. 2016.
- [9] P. Chen, Y. Bao, X. Zhu *et al.*, "Day-ahead scheduling of large numbers of thermostatically controlled loads based on equivalent energy storage model," *Journal of Modern Power Systems and Clean Energy*, vol. 7, no. 3, pp. 579-588, May 2019.
- [10] M. Q. Wang and H. B. Gooi, "Spinning reserve estimation in microgrids," *IEEE Transactions on Power Systems*, vol. 26, no. 3, pp. 1164-1174, Aug. 2011.
- [11] A. Cagnano, A. C. Bugliari, and E. D. Tuglie, "A cooperative control for the reserve management of isolated microgrids," *Applied Energy*, vol. 218, pp. 256-265, Mar. 2018.
- [12] H. Farzin, M. Fotuhi-Firuzabad, and M. Moeini-Aghaie, "A stochastic multi-objective framework for optimal scheduling of energy storage systems in microgrids," *IEEE Transactions on Smart Grid*, vol. 8, no. 1, pp. 117-127, Jan. 2017.
- [13] H. Farzin, M. Fotuhi-Firuzabad, and M. Moeini-Aghaie, "Stochastic energy management of microgrids during unscheduled islanding period," *IEEE Transactions on Industrial Informatics*, vol. 13, no. 3, pp. 1079-1087, Jun. 2017.
- [14] B. Li, M. Vrakopoulou, and J. L. Mathieu, "Chance constrained reserve scheduling using uncertain controllable loads part II: analytical reformulation," *IEEE Transactions on Smart Grid*, vol. 10, no. 2, pp. 1618-1625, Mar. 2019.
- [15] C. Qin and Y. Zeng, "SR-based chance-constrained economic dispatch for power systems with wind power," *IET Generation, Transmission & Distribution*, vol. 13, no. 13, pp. 2779-2788, Jul. 2019.
- [16] Z. Liu, J. Yang, Y. Zhang *et al.*, "Multi-objective coordinated planning of active-reactive power resources for decentralized droop-controlled islanded microgrids based on probabilistic load flow," *IEEE Access*, vol. 6, pp. 40267-40280, Jul. 2018.
- [17] B. Liu, K. Meng, Z. Y. Dong *et al.*, "Marginal bottleneck identification in power system considering correlated wind power prediction errors," *Journal of Modern Power Systems and Clean Energy*, vol. 8, no. 1, pp. 187-192, Jan. 2020.
- [18] B. Han, S. Lu, F. Xue *et al.*, "Day-ahead electric vehicle aggregator bidding strategy using stochastic programming in an uncertain reserve market," *IET Generation, Transmission & Distribution*, vol. 13, no. 12, pp. 2517-2525, Jun. 2019.
- [19] M. Xie, J. Xiong, S. Ke *et al.*, "Two-stage compensation algorithm for dynamic economic dispatching considering copula correlation of multi-wind farms generation," *IEEE Transactions on Sustainable Energy*, vol. 8, no. 2, pp. 763-771, Apr. 2017.
- [20] J. Yu, Z. Li, Y. Guo *et al.*, "Decentralized chance-constrained economic dispatch for integrated transmission-district energy systems," *IEEE Transactions on Smart Grid*, vol. 10, no. 6, pp. 6724-6734, Nov. 2019.
- [21] Y. Li, Z. Yang, G. Li *et al.*, "Optimal scheduling of an isolated microgrid with battery storage considering load and renewable generation uncertainties," *IEEE Transactions on Industrial Electronics*, vol. 66, no. 2, pp. 1565-1575, Feb. 2019.
- [22] T. Rodrigues, P. J. Ramirez, and G. Strbac, "Risk-averse bidding of energy and spinning reserve by wind farms with on-site energy storage," *IET Renewable Power Generation*, vol. 12, no. 2, pp. 165-173, Feb. 2018.
- [23] N. G. Paterakis, M. Gibescu, A. G. Bakirtzis *et al.*, "A multi-objective optimization approach to risk-constrained energy and reserve procurement using demand response," *IEEE Transactions on Power Systems*, vol. 33, no. 4, pp. 3940-3954, Jul. 2018.
- [24] M. Zhou, M. Wang, J. Li *et al.*, "Multi-area generation-reserve joint dispatch approach considering wind power cross-regional accommodation," *CSEE Journal of Power and Energy Systems*, vol. 3, no. 1, pp. 74-83, Mar. 2017.
- [25] M. Choudhry, *An Introduction to Value-at-risk*. Amsterdam: Wiley,

- 2012.
- [26] R. T. Rockafellar and S. Uryasev, "Conditional value-at-risk for general loss distributions," *Journal of Banking & Finance*, vol. 26, no. 7, pp. 1443-1447, Jul. 2002.
 - [27] Z. Chen, G. Zhu, Y. Zhang *et al.*, "Stochastic dynamic economic dispatch of wind-integrated electricity and natural gas systems considering security risk constraints," *CSEE Journal of Power and Energy Systems*, vol. 5, no. 3, pp. 324-334, Sept. 2019.
 - [28] S. Qaeini, M. S. Nazar, M. Yousefian *et al.*, "Optimal expansion planning of active distribution system considering coordinated bidding of downward active microgrids and demand response providers," *IET Renewable Power Generation*, vol. 13, no. 8, pp. 1291-1303, Jun. 2019.
 - [29] S. Moazeni, A. H. Miragha, and B. Defourny, "A risk-averse stochastic dynamic programming approach to energy hub optimal dispatch," *IEEE Transactions on Power Systems*, vol. 34, no. 3, pp. 2169-2178, May 2019.
 - [30] S. Das and M. Basu, "Day-ahead optimal bidding strategy of microgrid with demand response program considering uncertainties and outages of renewable energy resources," *Energy*, vol. 190, pp. 1-9, Jan. 2020.
 - [31] M. Vahedipour-Dahraie, A. Anvari-Moghaddam, and J. M. Guerrero, "Evaluation of reliability in risk-constrained scheduling of autonomous microgrids with demand response and renewable resources," *IET Renewable Power Generation*, vol. 12, no. 6, pp. 657-667, Apr. 2018.
 - [32] S. Bahramara, P. Sheikhamadi, and H. Golpira, "Co-optimization of energy and reserve in standalone micro-grid considering uncertainties," *Energy*, vol. 176, pp. 792-804, Jun. 2019.
 - [33] A. S. Farsangi, S. Hadayeghpars, M. Mehdinejad *et al.*, "A novel stochastic energy management of a microgrid with various types of distributed energy resources in presence of demand response programs," *Energy*, vol. 160, pp. 257-274, Oct. 2018.
 - [34] P. Li, D. Yu, M. Yang *et al.*, "Flexible look-ahead dispatch realized by robust optimization considering CVaR of wind power," *IEEE Transactions on Power Systems*, vol. 33, no. 5, pp. 5330-5340, Sept. 2018.
 - [35] P. Krokhmal, J. Palmquist, and S. Uryasev, "Portfolio optimization with conditional value-at-risk objective and constraints," *Journal of Risk*, vol. 4, no. 2, pp. 1-36, 2002.
 - [36] N. F. Avila and C. Chu, "Distributed probabilistic ATC assessment by optimality conditions decomposition and LHS considering intermittent wind power generation," *IEEE Transactions on Sustainable Energy*, vol. 10, no. 1, pp. 375-385, Jan. 2019.
 - [37] Y. Chen, J. Wen, and S. Cheng, "Probabilistic load flow method based on Nataf transformation and Latin hypercube sampling," *IEEE Transactions on Sustainable Energy*, vol. 4, no. 2, pp. 294-301, Apr. 2013.
 - [38] M. Mansour-Lakouraj and M. Shahabi, "Comprehensive analysis of risk-based energy management for dependent micro-grid under normal and emergency operations," *Energy*, vol. 171, pp. 928-943, Mar. 2019.
 - [39] N. Zhang, C. Kang, Q. Xia *et al.*, "A convex model of risk-based unit commitment for day-ahead market clearing considering wind power uncertainty," *IEEE Transactions on Power Systems*, vol. 30, no. 3, pp. 1582-1592, May 2015.
 - [40] Y. Fu and H. Chiang, "Toward optimal multiperiod network reconfiguration for increasing the hosting capacity of distribution networks," *IEEE Transactions on Power Delivery*, vol. 33, no. 5, pp. 2294-2304, Oct. 2018.
 - [41] A. Sujil, R. Kumar, and R. C. Bansal, "FCM clustering-ANFIS-based PV and wind generation forecasting agent for energy management in a smart microgrid," *The Journal of Engineering*, vol. 18, pp. 4852-4857, Jan. 2019.
 - [42] R. Mafakheri, P. Sheikhamadi, and S. Bahramara, "A two-level model for the participation of microgrids in energy and reserve markets using hybrid stochastic-IGDT approach," *International Journal of Electrical Power & Energy Systems*, vol. 119, pp. 105977, Jul. 2020.
 - [43] S. F. Gazijahani, A. Ajoulabadi, N. S. Ravadanegh *et al.*, "Joint energy and reserve scheduling of renewable powered microgrids accommodating price responsive demand by scenario: a risk-based augmented epsilon-constraint approach," *Journal of Cleaner Production*, vol. 262, pp. 1-10, Jul. 2020.
- Zehuai Liu** received the B.S. degree in electrical engineering from Guangdong University of Technology, Guangzhou, China, in 2011, and received the M.S. and Ph.D. degrees in electrical engineering from South China University of Technology, Guangzhou, China, in 2016 and 2020, respectively. His research interests include power system control and optimization, planning and operation of microgrids.
- Siliang Liu** received the B.S. and M.S. degrees in electrical engineering from South China University of Technology, Guangzhou, China, in 2016 and 2019, respectively. He is currently pursuing the Ph.D. degree in electrical engineering at South China University of Technology. His research interests include power system operation and planning.
- Qin hao Li** received the B.E. and Ph.D. degrees in electrical engineering from South China University of Technology, Guangzhou, China, in 2012 and 2018, respectively. He is currently working at South China University of Technology as a Postdoctoral Researcher. His research interest includes power system reactive power optimization.
- Yongjun Zhang** received the B.E. and Ph.D. degrees in electrical engineering from South China University of Technology, Guangzhou, China, in 1995 and 2004, respectively. From 1995 to 2005, he was a Research Assistant with the School of Electric Power, South China University of Technology, Guangzhou, China. From 2005 to 2012, he was an Associate Professor. Since 2012, he has been a Professor with the same school. His research interests include power system reactive power optimization, active distributed network, smart energy, and high-voltage direct current transmission.
- Wenyang Deng** received the B.S. degree in electrical engineering and its automation from Taiyuan University of Science and Technology, Taiyuan, China, in 2013, the M.S. degree in electrical power system engineering from University of Manchester, Manchester, U.K., in 2014, and the Ph.D. degree from University of Macau, Macao SAR, China, in 2020. His research interests include regulation of capacitive-coupling converter, power sharing of hybrid converter, and power quality improvement in microgrids.
- Lai Zhou** received the B.E. degree in electrical engineering from South China University of Technology, Guangzhou, China, in 2016, where she is currently pursuing the Ph.D. degree in electrical engineering with the School of Electric Power. Her research interests include operation and control of smart distributed network.